Inverse Optimal Robust Adaptive Controller for Upper Limb Rehabilitation Exoskeletons With Inertia and Load Uncertainties

Jiamin Wang, *Graduate Student Member, IEEE*, and Oumar R. Barry

***Abstract*—We propose a robust adaptive controller for the safe and accurate trajectory tracking control of upper limb rehabilitation exoskeletons. The proposed controller can adapt to the inertia and load uncertainties, and compensate for their effects. The H_∞ robustness of the controller in l_2 perturbation/disturbance attenuation is realized by nonlinear robust control theory via inverse optimality. We mathematically prove the asymptotic stability and optimality of the controller by stabilizing a Lyapunov function and minimizing a meaningful cost function, respectively. We then demonstrate the performance of the controller with the simulations of two different exoskeleton control systems. The results show that the controller can identify and compensate for model uncertainties, and realize good tracking performance in the presence of perturbations and disturbances. These qualities are crucial to the reliability and safety of exoskeleton operations. In addition to rehabilitation exoskeletons, the proposed framework can also be applied to the control of other multibody robotic systems.**

***Index Terms*—Optimization and optimal control, rehabilitation robotics, robust/adaptive control.**

NOMENCLATURE

The mathematical notations used are listed as following:

$\mathbf{F}\underline{(}\mathbf{Z}\underline{)}$	Single-Input function $\mathbf{F}$ with argument $\mathbf{Z}$ (to differentiate from multiplications of parenthesized terms)
$\Vert \mathbf{Z} \Vert_n$	n-norm of a matrix $\mathbf{Z}$ ($n = 2$ if not specified)
$\mathbf{c}_{m\times n}$	$m \times n$ matrix whose elements equal to $\mathbf{c} \in \mathbb{R}$ ($m,\ n$ fit with neighboring blocks if not specified)
$\mathbf{c}_m$	$m \times 1$ vector whose elements equal to $\mathbf{c} \in \mathbb{R}$
$\mathbf{I}_n$	Identity matrix of dimension n ($m,\ n$ fit with neighboring blocks if not specified)
$\mathrm{diag}\underline{(}\mathbf{z}\underline{)}$	Convert an m-dimensional vector $\mathbf{z}$ into an $m \times m$ diagonal matrix with elements from $\mathbf{z}$
$\mathbf{Z} > 0$	A square matrix $\mathbf{Z}$ is positive definite
$\mathbf{Z}^{+}$	The Moore-Penrose pseudo inverse of $\mathbf{Z}$
$\mathbf{Z}^{-\mathrm{T}}$	Transposed inverse of $\mathbf{Z}$ (since $(\mathbf{Z}^{-1})^{\mathrm{T}} = (\mathbf{Z}^{\mathrm{T}})^{-1}$)

Manuscript received October 13, 2020; accepted February 6, 2021. Date of publication February 23, 2021; date of current version March 11, 2021. This letter was recommended for publication by Associate Editor A. Quattrini Li and Editor L. Pallottino upon evaluation of the reviewers' comments. *(Corresponding author: Oumar Barry.)*

The authors are with the Department of Mechanical Engineering, Virginia Tech, Blacksburg, VA 24061 USA (e-mail: jmechw@vt.edu; obarry@vt.edu).

This letter has supplementary downloadable material available at https://doi.org/10.1109/LRA.2021.3061361, provided by the authors.

Digital Object Identifier 10.1109/LRA.2021.3061361

I. INTRODUCTION

In RECENT years, many mechatronic/robotic orthoses and exoskeletons have been developed to provide rehabilitation therapy and movement assistance for patients recovering from neurological disorders (e.g., strokes and pathological tremors) [1], [2]. Based on different designs for various applications, these rehabilitation devices are categorized as stationary (installed on a fixed/moving platform) [3]–[6] and wearable systems [7]–[9]. Provided that tracking references can be designed manually [10] or planned via voluntary motion prediction [11], [12], controllers are designed for the human-exoskeleton dynamical systems for trajectory tracking. The performance and stability of these controllers under model uncertainties, perturbations, and disturbances are crucial to the reliability and safety of exoskeleton operations.

The model reference adaptive controller (MRAC) is capable of compensating the dynamical model uncertainties [13]. Previous works investigated the application of MRAC in exoskeletons with inertia, force, and input uncertainties [6], [14], [15]. A few studies also take into consideration the robustness, and introduced robust adaptive sliding-mode controllers (SMC) that provide good motion tracking performance under uncertainties and disturbances [10], [16]. However, the gain switching controller in SMC can also lead to the chattering problem [17], which may damage the exoskeleton hardware and undermine the safety.

H_∞ controllers are popular optimal controllers with guaranteed robustness towards perturbations and disturbances [18], [19]. For nonlinear systems like exoskeletons, the design of an optimal controller can be challenging as it requires solving a Hamilton-Jacobi-Isaacs equation [20]. The existing algorithms such as the state-dependent Riccati equation cannot guarantee a globally optimal solution [21], [22]. For some problems, this challenge can be resolved by the inverse optimality technique, which produces a stabilizing controller later proven to be the global optimal solution of a meaningful cost function [19], [23]. Previous studies applied the inverse optimality technique to design robust adaptive controllers for spacecraft and robot manipulators [24]–[26]. However, these controllers may only apply to systems with specific model structures.

In this paper, for the first time, we propose an inverse optimal robust adaptive controller for upper limb rehabilitation exoskeletons. The controller design is established based on a generic model shared by a family of human-exoskeleton multibody systems. By combining MRAC and inverse optimal robust control (IORC) theories, the proposed inverse optimal robust adaptive controller (IO-RAC) can compensate for the effects of inertia and load uncertainties as well as providing H_∞ robustness in l_2 disturbance attenuation by optimizing a meaningful cost function. The proposed control framework applies to not only exoskeletons, but also other robotic systems.

The rest of the paper is arranged as follows: In Section II, we discuss the model and assumptions of the human-exoskeleton system to set up the control problem. Section III introduces the theory of IORC, then proposes the main result (i.e., IO-RAC) and discusses its properties. In Section IV, the performance of IO-RAC is demonstrated by simulations of a stationary exoskeleton and a wearable exoskeleton. Finally, Section V summarizes the finding and proposes future work. Detailed proofs of the stability and optimality of IO-RAC are included in Appendices A and B, respectively.

II. Problem Formulation

In this study, the proposed controller is designed for a family of upper limb rehabilitation exoskeletons that follow a generic human-exoskeleton multibody model structure:

$$\begin{aligned}\mathbf{M}(\mathbf{q},\mathbf{p}_a)\ddot{\mathbf{q}} = &-\mathbf{C}(\mathbf{q},\dot{\mathbf{q}},\mathbf{p}_a)\dot{\mathbf{q}} - \mathbf{h}(t,\mathbf{q},\dot{\mathbf{q}},\mathbf{p}_a,\mathbf{p}_b)\\ &+ \mathbf{J}_u^{\mathrm{T}}(\mathbf{q})\mathbf{u} + \mathbf{J}_w^{\mathrm{T}}(\mathbf{q})\mathbf{w}\end{aligned} \tag{1}$$

where $t \in \mathbb{R}_+$ is the time variable; $\mathbf{q} \in \mathbb{R}^{n_q}$ is the generalized coordinate; $\mathbf{u} \in \mathbb{R}^{n_u}$ is the control input from the exoskeleton; $\mathbf{w} \in \mathbb{R}^{n_w}$ is the bounded perturbation/disturbance; $\mathbf{M} \in \mathbb{R}^{n_q\times n_q}$ is the inertia matrix, which satisfies $\mathbf{M} = \mathbf{M}^{\mathrm{T}} > 0$; $\mathbf{C} \in \mathbb{R}^{n_q\times n_q}$ is the Coriolis and centripetal matrix; $\mathbf{h} \in \mathbb{R}^{n_q}$ is vector of the generalized forces, which includes potential energy forces and energy dissipation forces, and time-dependent excitations; $\mathbf{J}_u \in \mathbb{R}^{n_u\times n_q}$ is the control input Jacobian matrix; and $\mathbf{J}_w \in \mathbb{R}^{n_w\times n_q}$ is the disturbance input Jacobian matrix. Finally, $\mathbf{p}_a \in \mathbb{R}^{n_{p,a}}$ and $\mathbf{p}_b \in \mathbb{R}^{n_{p,b}}$ are the uncertain inertia and load parameters, respectively.

The model in Eq. (1) describes the dynamical interaction between user and exoskeleton based on a few model assumptions. When the user equips the exoskeleton, a close kinematic chain is formed between the coupling of human bodies and exoskeleton mechanisms, leading to the following assumptions:

1) The exoskeleton can actuate all the human degrees of freedom (DOF) within the closed kinematic chain, i.e, the human-exoskeleton system is fully-actuated. This leads to $n_u \geq n_q$ and $\mathrm{rank}(\mathbf{J}_u) = n_q$.
2) The soft body dynamics from the muscles and tissues in the musculoskeletal model is considered as perturbations within $\mathbf{w}$.
3) Uncertain loads from the user are generalized into direct forces/torques acting at the human joints, which are included in $\mathbf{h}$.

Following Assumption 1, a generalized control input $\mathbf{u}_c \in \mathbb{R}^{n_q}$ is introduced, whose relationship with $\mathbf{u}$ is

$$\mathbf{u}_c = \mathbf{J}_u^{\mathrm{T}}\mathbf{u}; \quad \mathbf{u} = (\mathbf{J}_u\mathbf{J}_u^{\mathrm{T}})^{-1}\mathbf{J}_u\mathbf{u}_c = \mathbf{J}_u^{+}\mathbf{u}_c \tag{2}$$

where Eq. (2) yields the $\mathbf{u}$ that has the smallest ℓ_2 norm according to the Moore-Penrose pseudo inverse.

Equation (1) also requires the uncertain parameter $\mathbf{p} = [\mathbf{p}_a^{\mathrm{T}},\ \mathbf{p}_b^{\mathrm{T}}]^{\mathrm{T}} \in \mathbb{R}^{n_p}$ (where $n_p = n_{p,a} + n_{p,b}$) to satisfy

$$\mathbf{M}(\mathbf{q},\mathbf{p}_a)\mathbf{z}_q = \mathbf{J}_M^{\mathrm{T}}(\mathbf{q},\mathbf{z}_q)\mathbf{p}_a + \mathbf{M}_0(\mathbf{q})\mathbf{z}_q \tag{3a}$$

$$\mathbf{C}(\mathbf{q},\dot{\mathbf{q}},\mathbf{p}_a)\mathbf{z}_q = \mathbf{J}_C^{\mathrm{T}}(\mathbf{q},\dot{\mathbf{q}},\mathbf{z}_q)\mathbf{p}_a + \mathbf{C}_0(\mathbf{q},\dot{\mathbf{q}})\mathbf{z}_q \tag{3b}$$

$$\mathbf{h}(t,\mathbf{q},\dot{\mathbf{q}},\mathbf{p}) = \mathbf{J}_h^{\mathrm{T}}(t,\mathbf{q},\dot{\mathbf{q}})\mathbf{p} + \mathbf{h}_0(t,\mathbf{q},\dot{\mathbf{q}}) \tag{3c}$$

where $\mathbf{z}_q \in \mathbb{R}^{n_q}$ is an arbitrary vector; $\mathbf{J}_M,\ \mathbf{J}_C \in \mathbb{R}^{n_{p,a}\times n_q}$, and $\mathbf{J}_h \in \mathbb{R}^{n_p\times n_q}$ are Jacobian matrices; $\mathbf{M}_0,\ \mathbf{C}_0 \in \mathbb{R}^{n_q\times n_q}$ and $\mathbf{h}_0 \in \mathbb{R}^{n_q}$ are the known parts of $\mathbf{M}$, $\mathbf{C}$, and $\mathbf{h}$, respectively. Specifically, Eq. (3) requires $\mathbf{p}_a$ to be selected as masses and moments of inertia only. These specifications also lead to two more assumptions:

4) The uncertain parameters are constant or slowly time-varying. This leads to $\dot{\mathbf{p}}_a \approx \mathbf{0}$ and $\dot{\mathbf{p}}_b \approx \mathbf{0}$.
5) The unknown kinematic parameters in the system can be estimated from motion measurements in real-time, which are then directly implemented in the controller design [6], [9]. The identification error leads to disturbances included in $\mathbf{w}$.

By introducing the time-dependent tracking reference $\mathbf{r}(t) \in \mathbb{R}^{n_q}$, the tracking error $\boldsymbol{\epsilon} \in \mathbb{R}^{n_q}$ and the state $\mathbf{x} \in \mathbb{R}^{n_x}$ (where $n_x = 2n_q$) of the control system can be written as

$$\boldsymbol{\epsilon} = \mathbf{q} - \mathbf{r}; \quad \mathbf{x} = \begin{bmatrix}\boldsymbol{\epsilon}^{\mathrm{T}} & \dot{\boldsymbol{\epsilon}}^{\mathrm{T}}\end{bmatrix}^{\mathrm{T}} \tag{4}$$

In some physiotherapies, $\mathbf{r}$ can be manually designed by the therapists [10]. The motion planning of $\mathbf{r}$ may also be realized through the extraction and prediction of voluntary motion [11], [12]. Hence, we propose a final assumption for this study:

6) The tracking reference $\mathbf{r}$ is smooth, bounded, and directly available. The discrepancy between $\mathbf{r}$ and user volition leads to disturbances included in $\mathbf{w}$.

Therefore, the control system can be written as

$$\dot{\mathbf{x}} = \mathbf{f}(\mathbf{x}) + \mathbf{g}(t,\mathbf{q},\dot{\mathbf{q}},\mathbf{p}) + \mathbf{U}(\mathbf{q})\mathbf{u}_c + \mathbf{W}(\mathbf{q})\mathbf{w} \tag{5}$$

where

$$\begin{aligned}&\mathbf{f} = \begin{bmatrix}\dot{\boldsymbol{\epsilon}} & \mathbf{0}\end{bmatrix}^{\mathrm{T}}; \quad \mathbf{g} = \begin{bmatrix}\mathbf{0} & \mathbf{M}^{-1}(-\mathbf{M}\ddot{\mathbf{r}} - \mathbf{C}\dot{\mathbf{q}} - \mathbf{h})\end{bmatrix}^{\mathrm{T}};\\ &\mathbf{U} = \begin{bmatrix}\mathbf{0} & \mathbf{M}^{-1}\end{bmatrix}^{\mathrm{T}}; \quad \mathbf{W} = \begin{bmatrix}\mathbf{0} & \mathbf{M}^{-1}\mathbf{J}_w^{\mathrm{T}}\end{bmatrix}^{\mathrm{T}}\end{aligned} \tag{6}$$

Hence, Eq. (5) is a time-dependent nonlinear control system affine in terms of both $\mathbf{u}_c$ and $\mathbf{w}$. An understatement for the assumptions is that the kinematic identification needs be reliable, and the motion planning of $\mathbf{r}$ cannot deviate far away from the user voluntary motion intention (or vice versa), so that $\mathbf{w}$ is bounded. Finally, Assumptions 1 and 4 are common assumptions applicable to not only exoskeletons, but also other robotic systems that fit in the generic model from Eq. (1).

III. Inverse Optimal Robust Adaptive Controller

This section first introduces the theoretical background of inverse optimal robust control (IORC). Then we propose the main result, i.e, the inverse optimal robust adaptive controller (IO-RAC) and discuss its properties.

A. Inverse Optimal Robust Control Theory

Here we introduce the theory of IORC [19], [23], [24]: For the control system in Eq. (5), with the uncertain parameters assumed as known constants $\mathbf{p} = \mathbf{p}_0 \in \mathbb{R}^{n_p}$, a smooth function $\mathcal{V}_0(\mathbf{x}, \mathbf{p}_0)$ is a robust control Lyapunov function, if there exists a controller $\mathbf{u}_{c,0}(t, \mathbf{x}, \mathbf{p}_0) \in \mathbb{R}^{n_q}$ smooth on $\mathbb{R}^{n_x} \times \mathbb{R}^{n_p}$ that satisfies $\mathbf{u}_{c,0}(\mathbf{0}, \mathbf{p}_0) = \mathbf{0}$, and a continuous function $Q_0(\mathbf{x}, \mathbf{p}_0) \geq 0$ ($Q_0 = 0$ iff. $\mathbf{x} = 0$) so that

$$(\partial \mathcal{V}_0/\partial \mathbf{x})(\mathbf{f} + \mathbf{g} + \mathbf{U}\mathbf{u}_{c,0} + \mathbf{W}\mathbf{w}_0) \leq -Q_0 \tag{7}$$

for the auxiliary control system of

$$\dot{\mathbf{x}} = \mathbf{f} + \mathbf{g} + \mathbf{U}\mathbf{u}_{c,0} + \mathbf{W}\mathbf{w}_0 \tag{8}$$

where

$$\mathbf{w}_0 = \ell_{\underline{\gamma}}\underline{(2\|\mathrm{L}_{\mathbf{W}}\mathcal{V}_0\|)}\left((\mathrm{L}_{\mathbf{W}}\mathcal{V}_0)^{\mathrm{T}}/\|\mathrm{L}_{\mathbf{W}}\mathcal{V}_0\|^2\right) \tag{9}$$

and $\gamma\underline{(\sigma)} \in \mathbb{R}_+$ is a class $\mathcal{K}_\infty$ function, whose derivative $\gamma'\underline{(\sigma)} = \partial\gamma/\partial\sigma$ is also a class $\mathcal{K}_\infty$ function. The function $\ell_{\underline{\gamma}}\underline{(\sigma)}$ denotes the Legendre-Fenchel transformation [23], [24]

$$\ell_{\underline{\gamma}}\underline{(\sigma)} = \sigma(\gamma')^{-1}\underline{(\sigma)} - \gamma\underline{((\gamma')^{-1}\underline{(\sigma)})} = \int_0^\sigma \left((\gamma')^{-1}\underline{(s)}\right) ds \tag{10}$$

and $\mathrm{L}_{\mathbf{W}}\mathcal{V}_0$ is the Lie derivative of $\mathcal{V}_0$ in terms of $\mathbf{W}$ (which is $\mathrm{L}_{\mathbf{W}}\mathcal{V}_0 = (\partial\mathcal{V}_0/\partial\mathbf{x})\mathbf{W}$).

Provided that there exists a function $\mathbf{R}_0(\mathbf{x}, \mathbf{p})$ that satisfies $\mathbf{R}_0 = \mathbf{R}_0^{\mathrm{T}} > 0$ so that $\mathbf{u}_{c,0}$ designed as

$$\mathbf{u}_{c,0} = -\mathbf{U}^{-1}\mathbf{g} + \mathbf{u}_{b,0}; \quad \mathbf{u}_{b,0} = -c_1\mathbf{R}_0^{-1}(\mathrm{L}_{\mathbf{U}}\mathcal{V}_0)^{\mathrm{T}} \tag{11}$$

with $c_1 = 1$ globally asymptotically stabilizes Eq. (8) with respect to $\mathcal{V}_0$. Then $\mathbf{u}_{c,0}$ solves the inverse optimal H_∞ control problem of Eq. (5) by minimizing the cost function

$$\begin{aligned}\mathcal{J}_0(\mathbf{u}_c) = \sup_{\mathbf{w}\in\mathbb{W}} \Bigg\{ \lim_{t\to\infty} \Bigg[2c_1\mathcal{V}_0 + \int_0^t \Bigg(&- 2c_1\mathrm{L}_{\mathbf{f}}\mathcal{V}_0 \\ - c_1c_2\ell_{\underline{\gamma}}\underline{(2\|\mathrm{L}_{\mathbf{W}}\mathcal{V}_0\|)} &+ c_1^2\mathrm{L}_{\mathbf{U}}\mathcal{V}_0\mathbf{R}_0^{-1}(\mathrm{L}_{\mathbf{U}}\mathcal{V}_0)^{\mathrm{T}} \\ + \mathbf{u}_{b,0}^{\mathrm{T}}\mathbf{R}_0\mathbf{u}_{b,0} - c_1c_2\gamma\underline{\left(\frac{\|\mathbf{w}\|}{c_2}\right)}\Bigg)dt\Bigg]\Bigg\}\end{aligned} \tag{12}$$

where $c_1 \geq 2$ and $c_2 \in (0, 2]$, and $\mathbb{W}$ is the set of locally bounded functions of $\mathbf{x}$; and $\mathrm{L}_{\mathbf{f}}\mathcal{V}_0$ and $\mathrm{L}_{\mathbf{U}}\mathcal{V}_0$ are the Lie derivatives: $\mathrm{L}_{\mathbf{f}}\mathcal{V}_0 = (\partial\mathcal{V}_0/\partial\mathbf{x})\mathbf{f}$ and $\mathrm{L}_{\mathbf{U}}\mathcal{V}_0 = (\partial\mathcal{V}_0/\partial\mathbf{x})\mathbf{U}$. For l_2 disturbance attenuation [23], [24], the γ function and its Legendre-Fenchel transformation can be selected as

$$\gamma\underline{(\sigma)} = \ell_{\underline{\gamma}}\underline{(2\sigma)} = \sigma^2 \tag{13}$$

In summary, the inverse optimal robust control is realized by proving that a stabilizing controller in Eq. (11) optimizes a cost function in Eq. (12). It is important to show that the cost function is meaningful for the validity of controller optimality. Also, note that Eq. (12) is designed only for IORC, which does not optimize the adaptive control process. Later in the paper, while the above process is referenced, a set of Lyapunov function and the cost function is specifically designed for the robust adaptive control problem in Eq. (5).

B. Main Result

A challenge in the synergy of model reference adaptive control (MRAC) and IORC arises from the model limitation. Robust adaptive controllers designed in previous studies [24]–[26] via inverse optimality only apply to specific models. Here we present the inverse optimal robust adaptive controller for the system in Eq. (5). The state controller $\mathbf{u}_c$ and updater of parameter estimate $\hat{\mathbf{p}} \in \mathbb{R}^{n_p}$ are

$$\mathbf{u}_c = \mathbf{J}_p^{\mathrm{T}}(t, \mathbf{q}, \dot{\mathbf{q}})\hat{\mathbf{p}} + \mathbf{u}_f(t, \mathbf{q}, \dot{\mathbf{q}}) + \mathbf{u}_b(t, \mathbf{x}) \tag{14a}$$

$$\dot{\hat{\mathbf{p}}} = -\boldsymbol{\Gamma}^{-1}\mathbf{J}_p(t, \mathbf{q}, \dot{\mathbf{q}})\boldsymbol{\xi} \tag{14b}$$

with the terms $\{\boldsymbol{\xi},\ \boldsymbol{\zeta},\ \mathbf{u}_f,\ \mathbf{u}_b\} \in \mathbb{R}^{n_q}$, $\mathbf{J}_p \in \mathbb{R}^{n_q\times n_p}$, and $\mathbf{R} \in \mathbb{R}^{n_q\times n_q}$ defined as

$$\boldsymbol{\xi} = \dot{\boldsymbol{\epsilon}} + \mathbf{K}_1\boldsymbol{\epsilon};\ \boldsymbol{\zeta} = \dot{\mathbf{r}} - \mathbf{K}_1\boldsymbol{\epsilon};\ \mathbf{R} = (\mathbf{J}_w^{\mathrm{T}}\mathbf{J}_w + \mathbf{K}_2)^{-1}; \tag{15a}$$

$$\mathbf{J}_p = \begin{bmatrix}\mathbf{J}_M^{\mathrm{T}}(\mathbf{q}, \dot{\boldsymbol{\zeta}}) + \mathbf{J}_C^{\mathrm{T}}(\mathbf{q}, \dot{\mathbf{q}}, \boldsymbol{\zeta}) & \mathbf{0}\end{bmatrix}^{\mathrm{T}} + \mathbf{J}_h^{\mathrm{T}}(t, \mathbf{q}, \dot{\mathbf{q}}); \tag{15b}$$

$$\mathbf{u}_f = \mathbf{M}_0\dot{\boldsymbol{\zeta}} + \mathbf{C}_0\boldsymbol{\zeta} + \mathbf{h}_0; \quad \mathbf{u}_b = -c_1\mathbf{R}^{-1}(t, \mathbf{x})\boldsymbol{\xi} \tag{15c}$$

where $\mathbf{K}_1,\ \mathbf{K}_2 \in \mathbb{R}^{n_q\times n_q}$, and $\boldsymbol{\Gamma} \in \mathbb{R}^{n_p\times n_p}$ are symmetric positive definite gain matrices. The design of $\mathbf{R} = \mathbf{R}^{\mathrm{T}} > 0$ in the feedback control term $\mathbf{u}_b$ provides H_∞ robustness via l_2 perturbation/disturbance attenuation. It should be noted that

$$\mathbf{J}_p^{\mathrm{T}}\mathbf{p} + \mathbf{u}_f = \mathbf{M}\dot{\boldsymbol{\zeta}} + \mathbf{C}\boldsymbol{\zeta} + \mathbf{h} \tag{16}$$

Therefore, $\mathbf{J}_p^{\mathrm{T}}\hat{\mathbf{p}}$ is the adaptive control term that compensates for inertial and load uncertainties via parameter estimates.

Apart from $\mathbf{J}_p$ determined by the model uncertainty structure, the performance of IO-RAC is determined by c_1, $\mathbf{K}_1$, $\mathbf{K}_2$, and $\mathbf{J}_w$. Specifically, c_1 scales the whole feedback controller $\mathbf{u}_b$; $\mathbf{K}_1$ determines the ratio between the gains of $\boldsymbol{\epsilon}$ and $\dot{\boldsymbol{\epsilon}}$; $\mathbf{K}_2$ sets the magnitudes of the fixed gain components; and $\mathbf{J}_w$, which is designed manually or based on system properties, decides the variable gain components for disturbance attenuation. The parameter estimate update rate is determined by $\boldsymbol{\Gamma}$. The proposed controller also does not require acceleration measurement or matrix inversion.

For any control parameters selected that follow their definitions, the proposed controller in Eq. (14) is globally asymptotically stable by converging a Lyapunov function

$$\mathcal{V}(\mathbf{x}, \hat{\mathbf{p}}) = \frac{1}{2}\mathbf{x}^{\mathrm{T}}\begin{bmatrix}\mathbf{K}_3 + \mathbf{K}_1\mathbf{M}\mathbf{K}_1 & \mathbf{K}_1\mathbf{M} \\ \mathbf{M}\mathbf{K}_1 & \mathbf{M}\end{bmatrix}\mathbf{x} + \frac{1}{2}\tilde{\mathbf{p}}^{\mathrm{T}}\boldsymbol{\Gamma}\tilde{\mathbf{p}} \tag{17}$$

where $\mathbf{K}_3 \in \mathbb{R}^{n_q\times n_q}$ is a positive definite matrix; and $\tilde{\mathbf{p}} = \hat{\mathbf{p}} - \mathbf{p} \in \mathbb{R}^{n_p}$ is the estimation error. The controller also provides l_2 disturbance attenuation by solving H_∞ control problem through minimizing a meaningful cost function:

$$\mathcal{J}(\mathbf{u}_c) = \sup_{\mathbf{w}\in\mathbb{W}} \left\{ \lim_{t\to\infty} \left[2c_1\mathcal{V} + \int_0^t \left(z_{J,1} - c_1c_2\gamma\left(\frac{\|\mathbf{w}\|}{c_2}\right) + \mathbf{u}_b^{\mathrm{T}}\mathbf{R}\mathbf{u}_b \right) dt \right] \right\} \quad (18)$$

where

$$z_{J,1}(\mathbf{x}) = -2c_1z_{J,2}(\mathbf{x}) - c_1c_2\ell_\gamma(2\|\mathrm{L}_\mathbf{W}\mathcal{V}\|) + c_1^2\mathrm{L}_\mathbf{U}\mathcal{V}\mathbf{R}^{-1}(\mathrm{L}_\mathbf{U}\mathcal{V})^{\mathrm{T}} \quad (19a)$$

$$z_{J,2}(\mathbf{x}) = \boldsymbol{\epsilon}\mathbf{K}_3\dot{\boldsymbol{\epsilon}} = \mathrm{L}_\mathbf{f}\mathcal{V} - \boldsymbol{\xi}^{\mathrm{T}}\mathbf{M}\mathbf{K}_1\dot{\boldsymbol{\epsilon}} \quad (19b)$$

The cost function penalizes both tracking error $\mathbf{x}$ and feedback control effort $\mathbf{u}_b$. Detailed proofs of the stability and optimality of IO-RAC are included in Appendices A and B, respectively.

Finally, while IO-RAC is designed to provide stable trajectory tracking for safe exoskeleton operations, the scope of the controller only lies in the dynamics of the human-exoskeleton system. For practical implementation, other safety concerns (e.g., range of motion, maximum velocity/acceleration, and input capacity) should also be taken into consideration during, for example, the motion planning of $\mathbf{r}$. In the next section, the performance of IO-RAC is demonstrated through two simulation case studies.

IV. Simulations and Discussions

This section demonstrates the performance of the robust adaptive controller from Eq. (14) through simulations of a stationary upper limb exoskeleton and a wearable wrist exoskeleton [9] carried out in MATLAB[1] [27]. For all simulations, the reference $\mathbf{r}$ and disturbance $\mathbf{w}$ are selected as bounded periodic and quasiperiodic trajectories with multiple harmonic components. The simulation sampling rate is 500 Hz, and the control input update rate is 250 Hz. The gravitational acceleration c_g is along the $-z$ axis of the global frame.

A. Stationary Exoskeleton

The 4-DOF stationary upper limb exoskeleton dynamical system is presented in Fig. 1. The conceptual design adopts a structure similar to the EXO-UL8 exoskeleton [5] without the forearm and wrist actuations. The joint of the ith link is labeled as θ_i, which is directly actuated by a motor torque input. When the user equips the exoskeleton, inertia and load uncertainties are introduced from the upper arm (Body 1) and forearm (Body 2) to Link 3 and Link 4, respectively. For the ith load, the unknown parameter $\mathbf{p}_i \in \mathbb{R}^7$ can be written as

$$\mathbf{p}_i = \begin{bmatrix} m_i & \boldsymbol{\phi}_i & \mathbf{c}_m \end{bmatrix}^{\mathrm{T}} \quad (20)$$

where m is the mass, $\boldsymbol{\phi} = [\phi_{xx},\ \phi_{yy},\ \phi_{zz}]^{\mathrm{T}}$ includes the moment of inertia elements in the local frame, and $\mathbf{c}_m = [c_{m,1},\ c_{m,2},\ c_{m,3}]^{\mathrm{T}}$ contains gravitational force parameters. To conveniently observe the convergence of parameter estimations, we simplify the inertia tensor to a diagonal matrix. With the

[1]The MATLAB codes for both simulations are available online at: https://github.com/VibRoLab-Group/IORAC_Exo

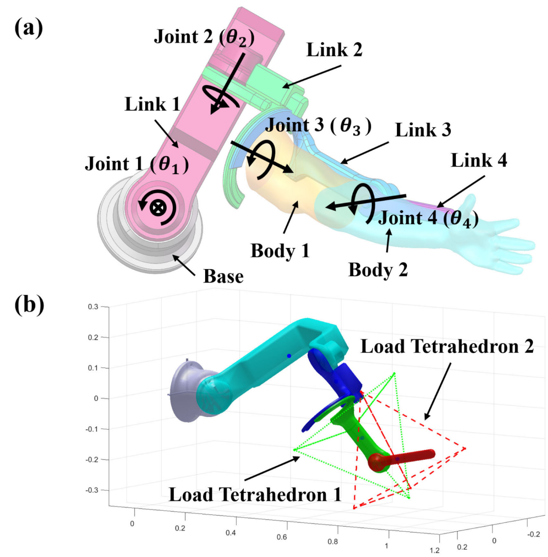

Fig. 1. The 3D model of the 4-DOF stationary exoskeleton with uncertain inertia and loads from the user is shown in (a). Body 1 and Body 2 are attached to link 3 and link 4, respectively; (b) shows the 3D model in the MATLAB environment, where the load tetrahedrons are used to identify the COM of the unknown bodies.

TABLE I
True Values of Uncertain Parameters and Default Controller Parameters for Stationary Robot Simulation

$m_1 = 3.80$ (kg)	$\boldsymbol{\phi}_1 = [0.18; 0.024; 0.17]$ (kg·m^2)
$m_2 = 4.50$ (kg)	$\boldsymbol{\phi}_2 = [0.87; 0.18; 1.03]$ (kg·m^2)
$\mathbf{d}_1 = [-5.6; 83; -2.7]$ (mm)	$\mathbf{d}_2 = [93.6; 174.6; -3.1]$ (mm)
$\mathbf{K}_1 = 4\ \mathbf{I}_4$ (1/s)	$\mathbf{K}_2 = 0.25\ \mathbf{I}_4$ (N·m·s/rad)
$c_1 = 2$	$\Lambda = \mathrm{diag}([1; \mathbf{1}\mathbf{0}_3; 1; \mathbf{1}\mathbf{0}_3; \mathbf{1}_6])/2$
$\mathbf{w} = \mathrm{diag}([3; 1; 3; 1])\ \mathbf{f}_w(t)$	$\mathbf{J}_w = 0.4\ \mathbf{J}_u\ \mathrm{diag}([3; 1; 3; 1])$

center of mass (COM) position of the uncertain body defined as $\mathbf{d}_i = [d_{i,x},\ d_{i,y},\ d_{i,z}]^{\mathrm{T}}$, $\mathbf{c}_{m,i}$ is introduced so that along with

$$c_{m,i,4} = m_i - (c_{m,i,1} + c_{m,i,2} + c_{m,i,3}) \quad (21)$$

each $c_{m,i,j}$ (j from 1 to 4) is a point mass that introduces a gravitational force component at a vertex of a load tetrahedron shown in Fig. 1(b). The load tetrahedron is located in the local frame of an uncertain body. Since gravitational forces are conservative in the global frame, the sum of all $c_{m,i,j}c_g$ will be the total gravitational force m_ic_g, and the weighted average of the translational positions of vertices by $c_{m,i,j}$ is the COM of the uncertain body.

The true values of uncertain parameters and default controller parameters are listed in Table I. We first test the controller by assuming no disturbance and only Body 2 is unknown. The initial estimation of $\mathbf{p}_2$ is set to $\hat{\mathbf{p}}_{2,t=0} = \mathbf{0}$. We also select $c_1 = 4$ and $\mathbf{J}_w = \mathbf{J}_u$ for this simulation. The tracking and parameter update trajectories are shown in Fig. 2. The tracking performances in Fig. 2(a–d) show that the trajectory can accurately follow the reference. The convergences of tracking errors of the four joints are presented in Fig. 2(e). Note that the startup behaviors of tracking errors can still be affected by model uncertainties since the parameter estimations are yet to converge. In application, this effect can be attenuated through accurate modeling of the known dynamical properties $\mathbf{M}_0$, $\mathbf{C}_0$, and $\mathbf{h}_0$ from Eq. (3). Figs. 2(f–h)

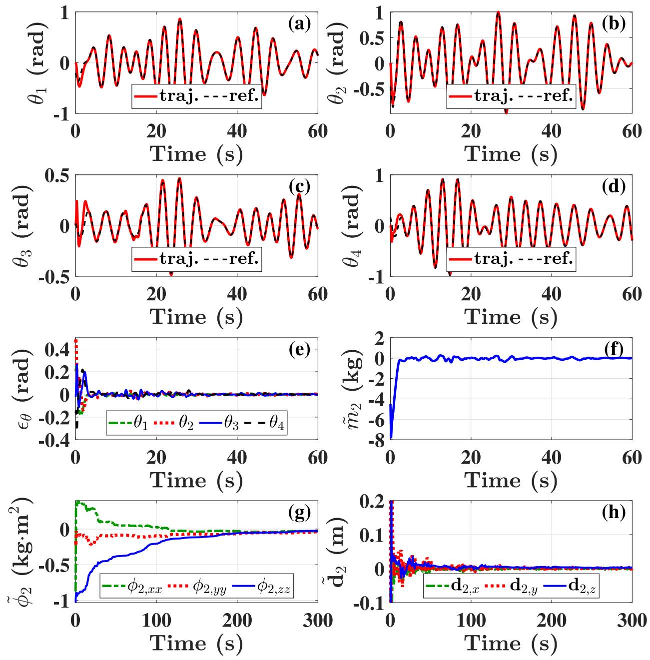

Fig. 2. Control performance of the stationary exoskeleton with uncertain Body 2 only. The comparisons between tracking trajectories and references of the four joints are shown in (a–d), respectively. The tracking errors $\boldsymbol{\epsilon}_\theta$ of the four joints are shown in (e). The estimation errors of uncertain parameters m_2, $\boldsymbol{\phi}_2$, and $\mathbf{d}_2$ are shown in (f–h), respectively.

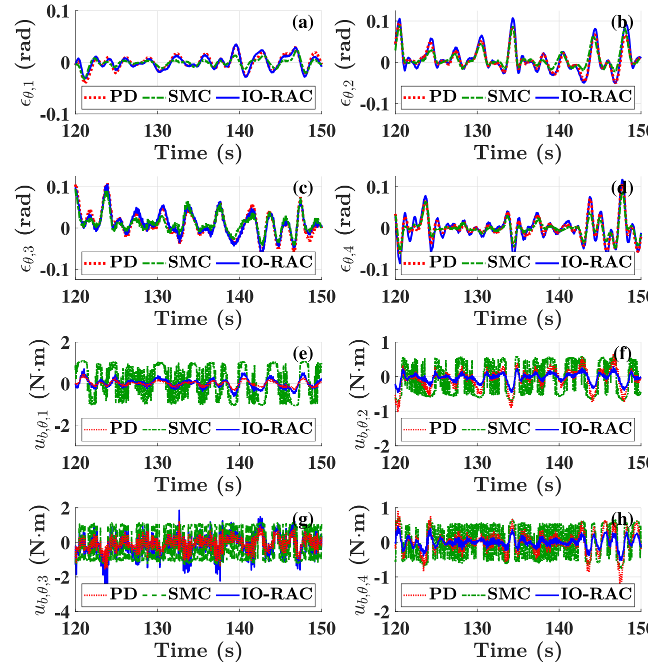

Fig. 4. Comparison of the stationary exoskeleton tracking controls with different feedback controller designs (i.e., PD, SMC, and IO-RAC). The time span starts at $t = 120$ second, so that the transient behaviors at the beginning of the simulation is diminished. The tracking errors (i.e., $\epsilon_{\theta,i}$) of the four joints (i.e., θ_i) are shown in (a–d), respectively. The feedback control inputs (i.e., $u_{c,\theta,i}$) at the four joints (i.e., θ_i) are shown in (e–h), respectively.

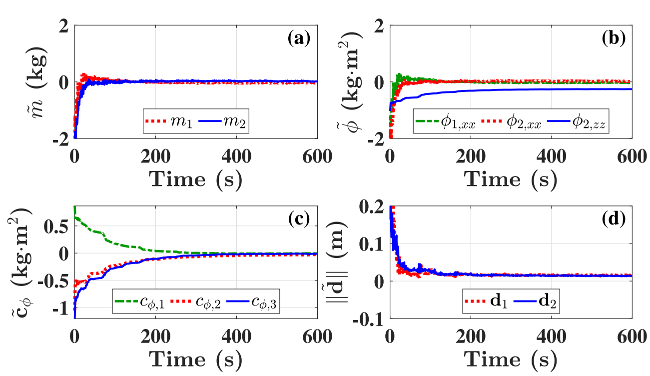

Fig. 3. Estimation errors of uncertain parameters from Body 1 and Body 2, where (a) presents $\tilde{m}_1$ and $\tilde{m}_2$, (b) shows $\tilde{\phi}_{1,xx}$, $\tilde{\phi}_{2,xx}$, and $\tilde{\phi}_{2,zz}$, (c) presents $\tilde{c}_{\phi,1}$, $\tilde{c}_{\phi,2}$, $\tilde{c}_{\phi,3}$, and (d) shows the 2-norm of $\tilde{\mathbf{d}}_1$ and $\tilde{\mathbf{d}}_2$.

show the convergences of all uncertain parameter estimation errors. It should be noted that the parameter update is driven by tracking errors. Since m_2 significantly affects the control performance, the quicker convergence of $\tilde{m}_2$ greatly reduces tracking errors, which results in $\tilde{\boldsymbol{\phi}}_2$ and $\tilde{\mathbf{d}}_2$ converging at a slower rate.

When both Body 1 and Body 2 are considered, uncertain parameter estimates do not converge to their true values. Fig. 3(b) shows that $\tilde{\phi}_{2,zz}$ does not converge to zero. By observing the symbolic structure of the inertia matrix $\mathbf{M}$ from Eq. (1), we notice that $\phi_{1,yy}$, $\phi_{2,zz}$, $\phi_{1,yy}$, and $\phi_{2,zz}$ do not distinctly affect $\mathbf{M}$. Instead, $\mathbf{M}$ is uniquely affected by a linear combination of these terms written as

$$\mathbf{c}_\phi = \begin{bmatrix} c_{\phi,1} \\ c_{\phi,2} \\ c_{\phi,3} \end{bmatrix} = \begin{bmatrix} \phi_{2,yy} - \phi_{2,zz} \\ \phi_{1,yy} + \phi_{2,zz} \\ \phi_{1,zz} + \phi_{2,zz} \end{bmatrix} \tag{22}$$

Therefore, we observe the convergence of $\tilde{\mathbf{c}}_\phi$ as shown in Fig. 3(c). The error in $\phi_{2,zz}$ also results in other estimates deviating from their truth, as shown in Fig. 3(a, d).

The above observations shows that uncertain parameter redundancy can result in estimates drifting from their truths. Also, the estimation convergence requires informative tracking references to "trigger" the distinct effects of uncertain parameters. However, the adaptive control term may manage to compensate for manifested model uncertainties without parameter estimation convergence. This can still lead to good tracking performance. In this case, since the estimation is error-driven, the parameter estimation convergence will also be slowed by the reduced tracking errors in return.

In the final test, we introduce the disturbance $\mathbf{w}$ overlaid on the control input, and adopts the default parameters in Table I. Note that the amplitudes of $\mathbf{f}_w(t) \in \mathbb{R}^4$ are amplified for disturbances on θ_1 and θ_3. We compare the performance of IO-RAC with two other adaptive controllers, whose feedback terms $\mathbf{u}_b$ are respectively selected as a proportional-derivative controller (PD), and a sliding mode controller (SMC) similar to those used in previous studies [10], [16]. Since all three controllers may obtain better disturbance attenuation with larger gains, we specifically configure the control parameters so that these controllers have similar performances as shown in Figs. 4(a–d). However, the feedback inputs from these controllers are significantly different.

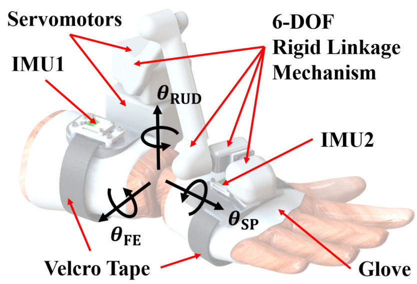

Fig. 5. The 3D design model of TAWE [9] on a right forearm with the major components labeled, where θ_{FE} is the approximate angle of flexion-extension, θ_{RUD} is the approximate angle of radial-ulnar deviation, and θ_{SP} is the approximate angle of supination-pronation.

From Figs. 4(f–h), we can observe the chattering, i.e., the rapid oscillations of feedback inputs in SMC caused by the gain switching control. This problem is less significant in the cases of PD and IO-RAC. Also, compared with PD, IO-RAC yields larger feedback inputs for θ_1 and θ_3, and significantly smaller input efforts for θ_2 and θ_4. This observation is expected since the design of $\mathbf{J}_w$ in IO-RAC takes into consideration the larger disturbances at θ_1 and θ_3, which is unlike the case of PD where simply large control gains are used ($\mathbf{u}_b$ for PD is designed as $\mathbf{u}_{b,\text{PD}} = -4c_1\mathbf{K}_2\boldsymbol{\xi}$). Therefore, with the reasonable design of $\mathbf{J}_w$, IO-RAC can potentially suppress disturbances at their origins, and prevent them from transmitting to other parts of the system.

The stationary exoskeleton example allows us to observe the fundamental behaviors of IO-RAC. The next case studies IO-RAC used in a wearable exoskeleton for tremor suppression.

B. Wearable Exoskeleton

Our team is developing TAWE [9] - a wearable wrist exoskeleton for active pathological tremor alleviation and movement assistance as shown in Fig. 5. TAWE features a 6-DOF rigid linkage mechanism that allows unconstrained wrist movement. Therefore, unlike the previous stationary exoskeleton case where the kinematics is defined by the exoskeleton mechanism, the kinematics of TAWE is defined by the biomechanism of the wrist. The detailed modeling of human-TAWE dynamics is explained and validated in [9]. For this study, we consider a simpler case where the forearm is fixed. This leads to the forearm being a 3-DOF system with $\mathbf{q}_1 = [\theta_{\text{RUD}},\ \theta_{\text{FE}},\ \theta_{\text{SP}}]^{\text{T}}$ as the wrist 3D rotation angles (i.e., radial-ulnar deviation (RUD), flexion-extension (FE), and supination-pronation (SP)), and TAWE being a 6-DOF system with $\mathbf{q}_2 \in \mathbb{R}^6$ as its six joints. With the closed kinematic chain formed between the forearm and TAWE, $\mathbf{q}_2$ are fully constrained to $\mathbf{q}_1$. Furthermore, since the wrist is a constrained 3D rotational joint, the rotation θ_{SP} on the SP direction is constrained to $\mathbf{q} = [\theta_{\text{RUD}},\ \theta_{\text{FE}}]^{\text{T}}$ [28]. The above configurations lead to a set of kinematic constraints defined as $\mathbf{r}_c(\mathbf{q}_1, \mathbf{q}_2) \in \mathbb{R}^7$, which constrains seven DOFs of the system in total. The time derivative of $\mathbf{r}_c$ can be calculated as

$$\dot{\mathbf{r}}_c = \mathbf{0} = \mathbf{J}_{c,q}(\mathbf{q}, \boldsymbol{\rho})\dot{\mathbf{q}} + \mathbf{J}_{c,\rho}(\mathbf{q}, \boldsymbol{\rho})\dot{\boldsymbol{\rho}}; \quad \boldsymbol{\rho} = \begin{bmatrix} \theta_{\text{SP}} & \mathbf{q}_2^{\text{T}} \end{bmatrix}^{\text{T}} \tag{23}$$

where $\mathbf{J}_{c,q} \in \mathbb{R}^{7\times 2}$ and $\mathbf{J}_{c,\rho} \in \mathbb{R}^{7\times 7}$ are Jacobian matrices ($\mathbf{J}_{c,\rho}$ is non-singular). Therefore, with $\dot{\boldsymbol{\rho}} = -\mathbf{J}_{c,\rho}^{-1}\mathbf{J}_{c,q}\dot{\mathbf{q}}$, we can obtain a 2-DOF assembled dynamical model that follows the dynamical

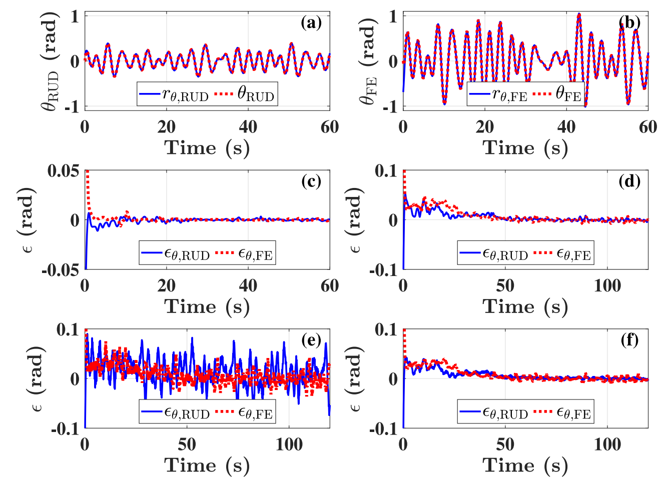

Fig. 6. The performances of the forearm-TAWE control system, where (a–b) shows the tracking trajectories (θ) and reference (r_θ) from the simulation with known human kinematics; (c) shows the tracking errors from the simulation with known human kinematics; (d) shows the tracking errors from the simulation with WKI algorithm; (e) shows the tracking errors from the simulation with tremor and WKI algorithm (passive tremor suppression); (e) shows the tracking errors from the simulation with tremor, WKI algorithm, and BMFLC (active tremor suppression).

model structure in Eq. (1). The control inputs are provided by the two servomotors at the first two joints of TAWE. The model uncertainties are the inertia and load from the hand. Similar to the stationary exoskeleton case, the uncertain parameter $\mathbf{p}$ is defined, and a load tetrahedron is established in the hand local frame (frame of IMU2).

By assuming that the wrist kinematics is known, we first test the tracking performance shown in Fig. 6. Observe from Fig. 6(a) that the trajectory of $\mathbf{q}$ is accurately following reference $\mathbf{r}$, and the errors in Fig. 6(b) converge quickly to zeros. These results confirm that the robust adaptive controller is applicable to the forearm-TAWE system.

In practice, the wrist kinematics is unknown. To solve this problem, we employ a wrist kinematic identification (WKI) algorithm via an extended Kalman filter [9], [29]. Based on the translational and rotational wrist motions measured by the inertia measurement units (IMU) and encoders on TAWE, the algorithm yields an approximated wrist model and estimates the wrist angle $\mathbf{q}_1$. The estimated wrist parameters and angle $\hat{\mathbf{q}}_1$ are used for the controller design. The second simulation indicates that the combination of IO-RAC and WKI algorithm is feasible. In the simulation, the WKI algorithm runs along with IO-RAC in the presence of disturbances and sensor noises. Due to both disturbance and estimation errors from WKI, the tracking errors shown in Fig. 6(d) have small oscillations. Since the performance is evaluated by the true $\mathbf{q}_1$ instead of its estimation $\hat{\mathbf{q}}_1$, the mean values of error oscillations may also slightly deviate from $\boldsymbol{\epsilon} = \mathbf{0}$.

Finally, we introduce the tremor as a model uncertainty. The synthetic tremor excitation is assumed to a combination of harmonic waves with different frequencies within a certain bandwidth (e.g., 3–6 Hz for Parkinsonian tremor [8]). For active tremor suppression, we designed a band-limited multi-frequency Fourier linear combiner (BMFLC) model, which is directly implemented as an adaptive control reference model for IO-RAC to compensate for the synthetic tremor [9], [30]. The comparison between passive (without BMFLC) and active tremor controls in Figs. 6(e–f) show that with a good bandwidth resolution, the implementation of BMFLC through IO-RAC can provide better tremor suppression as the error oscillation amplitudes are reduced.

In summary, the two simulations demonstrate that the proposed IO-RAC provides good performance and stability in the tracking control of rehabilitation exoskeletons with various model uncertainties and disturbances. The controller algorithms can run at 900 Hz on a 3.6 GHz CPU (AMD Ryzen 1800x), and potentially faster with code optimization.

V. Conclusion and Future Work

In this paper, we proposed a novel robust adaptive controller for upper limb rehabilitation exoskeletons. The controller is designed based on a general human-exoskeleton multibody model. By combining the model reference adaptive control and inverse optimal robust control theories, the proposed inverse optimal robust adaptive controller can compensate for inertia and load uncertainties, and provide H_∞ robustness in l_2 perturbation/disturbance attenuation. We mathematically proved the asymptotic stability of the controller by stabilizing a Lyapunov function. We also proved the optimality of the controller by showing that it minimizes a meaningful cost function. The proposed controller was then validated by the control simulations of the stationary exoskeleton and the TAWE systems. It was demonstrated that our controller can compensate for various inertia and load uncertainties, and provide good tracking stability and performance with the presence of disturbances. The controller can also be combined with identification algorithms for unknown human kinematics and applied for active tremor suppression. Hence, the proposed inverse optimal robust adaptive controller can be applied to safe and reliable motion control of rehabilitation exoskeletons. Finally, the proposed control framework applies to not only exoskeletons but also other robotic systems.

For future works, we will test the performance of the inverse optimal robust adaptive controller through experiments, and investigate the performance of the proposed controller with various motion planning algorithms. We will also explore the input-output robust adaptive controller design for under-actuated and nonholonomic systems so that it can be applied for a broader family of rehabilitation exoskeletons.

Appendix A
Lyapunov Stability of IO-RAC

Proof: The Lyapunov function in Eq. (17) is positive except $\mathcal{V}(\mathbf{0},\mathbf{p})=0$, which can be shown by rearranging $\mathcal{V}$ as

$$\mathcal{V}=(\boldsymbol{\xi}^{\mathrm{T}}\mathbf{M}\boldsymbol{\xi}+\boldsymbol{\epsilon}^{\mathrm{T}}\mathbf{K}_3\boldsymbol{\epsilon}+\tilde{\mathbf{p}}^{\mathrm{T}}\boldsymbol{\Gamma}\tilde{\mathbf{p}})/2 \tag{A-1}$$

Notice that the Lyapunov function is designed by utilizing the symmetric positive definiteness of $\mathbf{M}$. To obtain global asymptotic stability, it is required that the time-derivative $\dot{\mathcal{V}}<0$ except that $\dot{\mathcal{V}}(\mathbf{0},\mathbf{p})=0$. According to Assumption 4 in Section II, the time-derivative $\dot{\mathcal{V}}$ can be calculated as

$$\dot{\mathcal{V}}=\boldsymbol{\xi}^{\mathrm{T}}\mathbf{M}\dot{\boldsymbol{\xi}}+(\boldsymbol{\xi}^{\mathrm{T}}\dot{\mathbf{M}}\boldsymbol{\xi})/2+\boldsymbol{\epsilon}^{\mathrm{T}}\mathbf{K}_3\dot{\boldsymbol{\epsilon}}+\tilde{\mathbf{p}}^{\mathrm{T}}\boldsymbol{\Gamma}\dot{\tilde{\mathbf{p}}} \tag{A-2}$$

Based on Eq. (5), Eq. (A-2) can be transformed into

$$\begin{aligned}\dot{\mathcal{V}}=\ &\boldsymbol{\xi}^{\mathrm{T}}(-\mathbf{M}\ddot{\mathbf{r}}-\mathbf{C}\dot{\mathbf{q}}-\mathbf{h}+\mathbf{u}_c+\mathbf{J}_w^{\mathrm{T}}\mathbf{w}+\mathbf{M}\mathbf{K}_1\dot{\boldsymbol{\epsilon}})\\ &+(\boldsymbol{\xi}^{\mathrm{T}}\dot{\mathbf{M}}\boldsymbol{\xi})/2+\boldsymbol{\epsilon}^{\mathrm{T}}\mathbf{K}_3\dot{\boldsymbol{\epsilon}}+\tilde{\mathbf{p}}^{\mathrm{T}}\boldsymbol{\Gamma}\dot{\tilde{\mathbf{p}}}\end{aligned} \tag{A-3}$$

According to the Eq. (6) and Eq. (17), the Lie derivative of $\mathcal{V}$ with respect to $\mathbf{W}$ and $\mathbf{U}$ are respectively calculated as

$$\frac{\partial\mathcal{V}}{\partial\mathbf{x}}=\mathbf{x}^{\mathrm{T}}\begin{bmatrix}\mathbf{K}_3+\mathbf{K}_1\mathbf{M}\mathbf{K}_1 & \mathbf{K}_1\mathbf{M}\\ \mathbf{M}\mathbf{K}_1 & \mathbf{M}\end{bmatrix} \tag{A-4a}$$

$$\mathrm{L}_{\mathbf{W}}\mathcal{V}=\boldsymbol{\xi}^{\mathrm{T}}\mathbf{J}_w^{\mathrm{T}};\quad \mathrm{L}_{\mathbf{U}}\mathcal{V}=\boldsymbol{\xi}^{\mathrm{T}} \tag{A-4b}$$

Based on the auxiliary system in Eq. (8) and the gamma function selection from Eq. (13), the l_2 perturbation/disturbance attenuation assumes that the perturbation/disturbance $\mathbf{w}_{0,L\text{-}2}$ is bounded by $\mathbf{x}$ through

$$\mathbf{w}_{0,L\text{-}2}=\ell_\gamma\underline{(}2\|\mathrm{L}_{\mathbf{W}}\mathcal{V}\|\underline{)}\left((\mathrm{L}_{\mathbf{W}}\mathcal{V})^{\mathrm{T}}/\|\mathrm{L}_{\mathbf{W}}\mathcal{V}\|^2\right)=\mathbf{J}_w\boldsymbol{\xi} \tag{A-5}$$

Hence, bringing $\mathbf{u}_c$ from Eq. (14a) and $\mathbf{w}=\mathbf{w}_{0,L\text{-}2}$ from Eq. (A-5) into Eq. (A-3) yields

$$\begin{aligned}\dot{\mathcal{V}}=\ &\boldsymbol{\xi}^{\mathrm{T}}(-c_1\mathbf{R}^{-1}+\mathbf{J}_w^{\mathrm{T}}\mathbf{J}_w)\boldsymbol{\xi}+\left(\boldsymbol{\xi}^{\mathrm{T}}(\dot{\mathbf{M}}-2\mathbf{C})\boldsymbol{\xi}\right)/2\\ &+\boldsymbol{\epsilon}^{\mathrm{T}}\mathbf{K}_3\dot{\boldsymbol{\epsilon}}+\tilde{\mathbf{p}}^{\mathrm{T}}\boldsymbol{\Gamma}\left(\dot{\tilde{\mathbf{p}}}+\boldsymbol{\Gamma}^{-1}\mathbf{J}_p\boldsymbol{\xi}\right)\end{aligned} \tag{A-6}$$

Note that for a multibody system, $\dot{\mathbf{M}}-2\mathbf{C}$ is a skew matrix [10] so that $\boldsymbol{\xi}^{\mathrm{T}}(\dot{\mathbf{M}}-2\mathbf{C})\boldsymbol{\xi}=0$. Finally, by inserting the expressions of $\dot{\mathbf{p}}$ and $\mathbf{R}^{-1}$ respectively from Eq. (14b) and Eq. (15a), Eq. (A-6) is transformed into

$$\begin{aligned}\dot{\mathcal{V}}=\ &\boldsymbol{\xi}^{\mathrm{T}}\mathbf{J}_w^{\mathrm{T}}\mathbf{J}_w\boldsymbol{\xi}+\boldsymbol{\epsilon}^{\mathrm{T}}\mathbf{K}_3\dot{\boldsymbol{\epsilon}}-c_1\boldsymbol{\xi}^{\mathrm{T}}\mathbf{R}^{-1}\boldsymbol{\xi}\\ =\ &-(c_1-1)\boldsymbol{\xi}^{\mathrm{T}}\mathbf{J}_w^{\mathrm{T}}\mathbf{J}_w\boldsymbol{\xi}-c_1\boldsymbol{\xi}^{\mathrm{T}}(\mathbf{K}_2-\mathbf{K}_4/c_1)\boldsymbol{\xi}\\ &-\dot{\boldsymbol{\epsilon}}^{\mathrm{T}}\mathbf{K}_4\dot{\boldsymbol{\epsilon}}-\boldsymbol{\epsilon}^{\mathrm{T}}\mathbf{K}_1\mathbf{K}_4\mathbf{K}_1\boldsymbol{\epsilon}\end{aligned} \tag{A-7}$$

where $\mathbf{K}_4\in\mathbb{R}^{n_q\times n_q}$. It is required that $(\mathbf{K}_2-\mathbf{K}_4/c_1)>0$, and: (1) $\mathbf{K}_4=\mathbf{I}_{n_q}/2$ for $\mathbf{K}_1=\mathbf{K}_3$; or (2) $\mathbf{K}_4=\mathbf{K}_1^{-1}\mathbf{K}_3/2=\mathbf{K}_3\mathbf{K}_1^{-1}/2$ for diagonal $\mathbf{K}_1$ and $\mathbf{K}_3$ matrices. Thus, with any $c_1\geq 2$, there exists a smooth function $Q\underline{(}\mathbf{x}\underline{)}\geq 0$ ($Q=0$ iff. $\mathbf{x}=\mathbf{0}$) so that

$$\dot{\mathcal{V}}\leq -Q \tag{A-8}$$

and $\dot{\mathcal{V}}=-Q$ iff. $\mathbf{x}=\mathbf{0}$. Hence, IO-RAC from Eq. (14) globally asymptotically can stabilize the control system in Eq. (5) by converging the Lyapunov function in Eq. (17).

Appendix B
Optimality of IO-RAC

Proof: The cost function $\mathcal{J}$ in Eq. (18) is slightly different from $\mathcal{J}_0$ in Eq. (12). The difference lies in $z_{J,2}$ from Eq. (19b), where the term $\boldsymbol{\xi}^{\mathrm{T}}\mathbf{M}\mathbf{K}_1\dot{\boldsymbol{\epsilon}}$ originally contained in $\mathrm{L}_{\mathbf{f}}\mathcal{V}$ by the adaptive control term. However, the $\mathcal{J}$ can still be proved meaningful. Based on Eq. (13) and Eq. (A-4b), it can be observed from Eq. (A-7) that

$$\dot{\mathcal{V}}=z_{J,2}+\ell_\gamma\underline{(}2\|\mathrm{L}_{\mathbf{W}}\mathcal{V}\|\underline{)}-c_1\mathrm{L}_{\mathbf{U}}\mathcal{V}\mathbf{R}^{-1}(\mathrm{L}_{\mathbf{U}}\mathcal{V})^{\mathrm{T}} \tag{A-9}$$

With $c_1\geq 2$ and $c_2\in(0,2]$, according to Eq. (19a) and Eq. (A-8), it can be obtained that

$$\begin{aligned}z_{J,1}\underline{(}\mathbf{x}\underline{)}=\ &-2c_1\dot{\mathcal{V}}+c_1(2-c_2)\ell_\gamma\underline{(}2\|\mathrm{L}_{\mathbf{W}}\mathcal{V}\|\underline{)}\\ &+c_1(c_1-2)\mathrm{L}_{\mathbf{U}}\mathcal{V}\mathbf{R}^{-1}(\mathrm{L}_{\mathbf{U}}\mathcal{V})^{\mathrm{T}}\geq Q\end{aligned} \tag{A-10}$$

and $z_{J,1}=0$ iff. $\mathbf{x}=\mathbf{0}$. Therefore, $\mathcal{J}$ is a meaningful cost function [23], [24], since the positive definite term $z_{J,1}$ penalizes large tracking error $\mathbf{x}$, and the positive definite term $\mathbf{u}_b^{\mathrm{T}}\mathbf{R}\mathbf{u}_b$ penalizes large feedback control effort $\mathbf{u}_b$. The trade-off between tracking error and input effort can be adjusted by control parameters (i.e., $\mathbf{K}_1$, $\mathbf{K}_2$, and $\mathbf{J}_w$).

To prove that the proposed controller in Eq. (14) optimizes the cost function $\mathcal{J}$, based on $\boldsymbol{\xi}^{\mathrm{T}}(\dot{\mathbf{M}} - 2\mathbf{C})\boldsymbol{\xi} = 0$, we first obtain from Eq. (14) and Eq. (A-3) that

$$z_{J,2} = \Big(\dot{\mathcal{V}} - \boldsymbol{\xi}^{\mathrm{T}}(-\mathbf{M}\zeta - \mathbf{C}\zeta - \mathbf{h} + \mathbf{J}_p^{\mathrm{T}}\hat{\mathbf{p}} + \mathbf{u}_f + \mathbf{J}_w^{\mathrm{T}} + \mathbf{u}_b\mathbf{w}) - \tilde{\mathbf{p}}^{\mathrm{T}}\boldsymbol{\Gamma}\dot{\hat{\mathbf{p}}}\Big) = \dot{\mathcal{V}} - \boldsymbol{\xi}^{\mathrm{T}}(\mathbf{u}_b + \mathbf{J}_w^{\mathrm{T}}\mathbf{w}) \quad \text{(A-11)}$$

With Eq. (13), Eq. (A-4b), and Eq. (A-11), Eq. (18) can be transformed into

$$\begin{aligned}\mathcal{J}(\mathbf{u}_c) = &\sup_{\mathbf{w}\in\mathbb{W}}\Bigg\{\lim_{t\to\infty}\Bigg[2c_1\mathcal{V} + \int_0^t\Bigg(-2c_1\dot{\mathcal{V}} - \frac{c_1\mathbf{w}^{\mathrm{T}}\mathbf{w}}{c_2} \\ &+ 2c_1\boldsymbol{\xi}^{\mathrm{T}}(\mathbf{u}_b + \mathbf{J}_w^{\mathrm{T}}\mathbf{w}) - c_1c_2\boldsymbol{\xi}^{\mathrm{T}}\mathbf{J}_w^{\mathrm{T}}\mathbf{J}_w\boldsymbol{\xi} \\ &+ c_1^2\boldsymbol{\xi}^{\mathrm{T}}\mathbf{R}^{-1}\boldsymbol{\xi}^{\mathrm{T}} + \mathbf{u}_b^{\mathrm{T}}\mathbf{R}\mathbf{u}_b\Bigg)dt\Bigg]\Bigg\} \\ = &\; 2c_1\mathcal{V}(\mathbf{x}_{t=0}, \hat{\mathbf{p}}_{t=0}) + \sup_{\mathbf{w}\in\mathbb{W}}\Bigg\{\lim_{t\to\infty}\Bigg[\int_0^t\Bigg(z_{J,3} \\ &- c_1c_2\left\|\frac{\mathbf{w}}{c_2} - \mathbf{w}_{0,L\text{-}2}\right\|^2(\mathbf{x})\Bigg)dt\Bigg]\Bigg\} \qquad \text{(A-12)}\end{aligned}$$

where

$$z_{J,3} = (\mathbf{u}_b + c_1\mathbf{R}^{-1}\boldsymbol{\xi})^{\mathrm{T}}\mathbf{R}(\mathbf{u}_b + c_1\mathbf{R}^{-1}\boldsymbol{\xi}) \quad \text{(A-13)}$$

With $\mathbf{u}_b$ from Eq. (15c), we can obtain $z_{J,3} = 0$. Equation (A-12) also shows that the maximum value of Lyapunov function $\mathcal{V}(\mathbf{x}_{t=0}, \hat{\mathbf{p}}_{t=0})$ is obtained at $t = 0$, which indicates the convergence of $\mathcal{V}$ over time. Finally, it can be proved that

$$\Upsilon = \sup_{\mathbf{w}\in\mathbb{W}}\left\{\int_0^\infty\left(-c_1c_2\left\|\frac{\mathbf{w}}{c_2} - \mathbf{w}_{0,L\text{-}2}\right\|^2\right)dt\right\} \le 0 \quad \text{(A-14)}$$

and Υ reaches $\Upsilon = 0$ iff. $\mathbf{w} = c_2\mathbf{w}_{0,L\text{-}2} = c_2\mathbf{J}_w\boldsymbol{\xi}$, which is the worst-case disturbance [23], [24]. Hence, IO-RAC from Eq. (14) can provide l_2 disturbance attenuation by solving H_∞ control problem through minimizing the cost function $\mathcal{J}$.

References

[1] P. Maciejasz, J. Eschweiler, K. Gerlach-Hahn, A. Jansen-Troy, and S. Leonhardt, "A survey on robotic devices for upper limb rehabilitation," *J. Neuroengineering Rehabil.*, vol. 11, no. 1, pp. 1–29, 2014.

[2] N. P. Fromme, M. Camenzind, R. Riener, and R. M. Rossi, "Need for mechanically and ergonomically enhanced tremor-suppression orthoses for the upper limb: A systematic review," *J. Neuroengineering Rehabil.*, vol. 16, no. 1, pp. 1–15, 2019.

[3] C. G. Rose, E. Pezent, C. K. Kann, A. D. Deshpande, and M. K. O'Malley, "Assessing wrist movement with robotic devices," *IEEE Trans. Neural Syst. Rehabil. Eng.*, vol. 26, no. 8, pp. 1585–1595, Aug. 2018.

[4] J. C. Perry, J. Rosen, and S. Burns, "Upper-limb powered exoskeleton design," IEEE/*ASME Trans. Mechatronics*, vol. 12, no. 4, pp. 408–417, Aug. 2007.

[5] Y. Shen, P. W. Ferguson, J. Ma, and J. Rosen, "Chapter 4 - upper limb wearable exoskeleton systems for rehabilitation: State of the art review and a case study of the exo-ul8—dual-arm exoskeleton system," in *Wearable Technology in Medicine and Health Care*, R. K.-Y. Tong, Ed. Academic Press, 2018, pp. 71–90.

[6] B. Brahmi, M. Saad, J. T. A. T. Lam, C. O. Luna, P. S. Archambault, and M. H. Rahman, "Adaptive control of a 7-DOF exoskeleton robot with uncertainties on kinematics and dynamics," *Eur. J. Control*, vol. 42, pp. 77–87, 2018.

[7] R. C. Loureiro, J. M. Belda-Lois, E. R. Lima, J. L. Pons, J. J. Sanchez-Lacuesta, and W. S. Harwin, "Upper limb tremor suppression in ADL via an orthosis incorporating a controllable double viscous beam actuator," in *Proc. 9th Int. Conf. Rehabil. Robot.*, 2005, pp. 119–122.

[8] E. Rocon, J. Belda-Lois, A. Ruiz, M. Manto, J. C. Moreno, and J. L. Pons, "Design and validation of a rehabilitation robotic exoskeleton for tremor assessment and suppression," *IEEE Trans. Neural Syst. Rehabil. Eng.*, vol. 15, no. 3, pp. 367–378, Sep. 2007.

[9] J. Wang and O. Barry, "Multibody analysis and control of a full-wrist exoskeleton for tremor alleviation," *J. Biomechanical Eng.*, 2020, Art. no. 121008.

[10] B. Brahmi, A. Brahmi, M. Saad, G. Gauthier, and M. Habibur Rahman, "Robust adaptive tracking control of uncertain rehabilitation exoskeleton robot," *J. Dyn. Syst., Meas., Control*, vol. 141, no. 12, 2019, Art. no. 121007.

[11] J. A. Gallego, E. Rocon, J. O. Roa, J. C. Moreno, and J. L. Pons, "Real-time estimation of pathological tremor parameters from gyroscope data," *Sensors*, vol. 10, no. 3, pp. 2129–2149, 2010.

[12] Y. Matsumoto *et al.*, "Tremor frequency based filter to extract voluntary movement of patients with essential tremor," in *Proc. 4th IEEE RAS EMBS Int. Conf. Biomed. Robot. Biomechatronics*, 2012, pp. 1415–1422.

[13] M. Krstic, P. V. Kokotovic, and I. Kanellakopoulos, *Nonlinear and Adaptive Control Design*. Hoboken, NJ, USA: John Wiley & Sons, Inc., 1995.

[14] X. Wang, X. Li, J. Wang, X. Fang, and X. Zhu, "Data-driven model-free adaptive sliding mode control for the multi degree-of-freedom robotic exoskeleton," *Inf. Sci.*, vol. 327, pp. 246–257, 2016.

[15] W. He, Z. Li, Y. Dong, and T. Zhao, "Design and adaptive control for an upper limb robotic exoskeleton in presence of input saturation," *IEEE Trans. Neural Netw. Learn. Syst.*, vol. 30, no. 1, pp. 97–108, Jan. 2018.

[16] F. Cao, C. Li, and Y. Li, "Robust sliding mode adaptive control for lower extremity exoskeleton," in *Proc. Chin. Automat. Congr.*, 2015, pp. 400–405.

[17] V. Utkin and H. Lee, "Chattering problem in sliding mode control systems," in *Proc. Int. Workshop Variable Struct. Syst.*, 2006, pp. 346–350.

[18] R. Freeman and P. V. Kokotovic, *Robust Nonlinear Control Design: State-Space and Lyapunov Techniques*. Berlin, Germany: Springer Science & Business Media, 2008.

[19] M. Krstic and H. Deng, *Stabilization of Nonlinear Uncertain Systems*. Springer London, 1998.

[20] M. Aliyu, *Nonlinear H-Infinity Control, Hamiltonian Systems and Hamilton-Jacobi Equations*. Boca Raton, FL, USA: CRC Press, 2017.

[21] J. R. Cloutier, "State-Dependent Riccati equation techniques: An overview," in *Proc. Amer. Control Conf.*, vol. 2, 1997, pp. 932–936.

[22] M. Xin and S. Balakrishnan, "A new method for suboptimal control of a class of non-linear systems," *Optimal Control Appl. Methods*, vol. 26, no. 2, pp. 55–83, 2005.

[23] M. Krstic and Z.-H. Li, "Inverse optimal design of input-to-state stabilizing nonlinear controllers," *IEEE Trans. Autom. Control*, vol. 43, no. 3, pp. 336–350, Mar. 1998.

[24] W. Luo, Y.-C. Chu, and K.-V. Ling, "Inverse optimal adaptive control for attitude tracking of spacecraft," *IEEE Trans. Autom. Control*, vol. 50, no. 11, pp. 1639–1654, Nov. 2005.

[25] K. Sato, T. Nakashima, and K. Tsuruta, "A robust adaptive H-∞ control for robotic manipulators with input torque uncertainties," *Int. J. Adv. Mechatronic Syst.*, vol. 1, no. 2, pp. 116–124, 2008.

[26] R. Hayat, M. Leibold, and M. Buss, "Robust-adaptive controller design for robot manipulators using the H-∞ approach," *IEEE Access*, vol. 6, pp. 51 626–51 639, 2018.

[27] J. Wang, V. R. Kamidi, and P. Ben-Tzvi, "A multibody toolbox for hybrid dynamic system modeling based on nonholonomic symbolic formalism," in *Proc. ASME Dyn. Syst. Control Conf. Amer. Soc. Mech. Eng.*, 2018, pp. V00 3T29A003–V003T29A003.

[28] Z.-M. Li, L. Kuxhaus, J. A. Fisk, and T. H. Christophel, "Coupling between wrist flexion-extension and radial-ulnar deviation," *Clin. Biomech.*, vol. 20, no. 2, pp. 177–183, 2005.

[29] S. S. Haykin, *Adaptive Filter Theory*. Harlow, U.K.: Pearson Education Ltd.,2005.

[30] K. C. Veluvolu and W. T. Ang, "Estimation of physiological tremor from accelerometers for real-time applications," *Sensors*, vol. 11, no. 3, pp. 3020–3036, 2011.